PERGAMON

Chemical Engineering Science 55 (2000) 3175–3185

Chemical Engineering Science

Measurements and model prediction of the solid–liquid equilibria of organic binary mixtures

Cheng-Chia Huang, Yan-Ping Chen*

Department of Chemical Engineering, National Taiwan University, Taipei, Taiwan

Received 12 July 1999; received in revised form 22 November 1999; accepted 29 November 1999

Abstract

Solid–liquid equilibria of three binary mixtures consisting of benzoic acid, 2-aminobenzoic acid and 1-naphthol were measured in this study using differential scanning calorimetry (DSC). Simple eutectic phase diagrams were observed, and the experimental data were well correlated by either the Wilson equation or the UNIFAC activity coefficient model. A new method by employing the DSC experiment and the theoretical calculations to detect the fractional transformation of solid–liquid equilibrium of organic mixture is proposed. Deconvolution method was employed to obtain the ideal equilibrium solid–liquid DSC curve. The heat generation rate and fraction of transformation were calculated using the Gray's model. Applying this theoretical approach, the eutectic points and the equilibrium liquidus temperatures were easily determined from the fractional transformation curve. An easier procedure to confirm the composition of eutectic point is presented. It is also demonstrated that the solid–liquid equilibrium phase boundaries are predicted with good agreement to the experimental results.

Keywords: Deconvolution method; Heat transfer; Mathematical modelling; Phase equilibria; Thermodynamics

1. Introduction

Solid–liquid equilibrium (SLE) data are essential to the design of the purification process for specialty chemicals. Besides the traditional technique of cooling curve and visual measurement (Jakob, Joh, Rose & Gmehling, 1995), the differential scanning calorimetry (DSC) method is also used in many experimental studies on metal, polymer and organic compounds (e.g. Smith & Pennings, 1974; Matsuoka & Ozawa, 1989; Frezzotti, Bonifaci, Cavalca, Malaguti & Ravanetti, 1993; Santilli, Filippis & Chianese, 1994; Hammami & Mehrotra, 1995; Floter, Hollanders, de Loos & de Swaan Arons, 1997). DSC provides a useful technique for determining the phase boundaries through the measurement of heat effect during the phase transformation process (Hammami & Mehrotra, 1992).

Several mathematical models for either the DSC or differential thermal analysis (DTA) curve have been presented. Gray (1968) proposed a heat transfer modeling for the thermal analysis cell. Sarge, Bauerecker and Cammenga (1988) presented a resistance-capacity model for a heat flux calorimeter. Hemminger and Sarge (1991) applied a mathematical model to determine the baseline construction for a DSC curve. Ciach, Kapturkiewiza, Wolczynski and Zahra (1992) also gave a mathematical treatment for the heat flux of DSC and employed the results to explain the metal solidification. Based on the Gray's model, the relationship between the peak shape of a DTA curve and the shape of a phase diagram has been discussed by Chen, Huang and Lin (1995). In many cases, the area shown between a DSC curve and its baseline is taken as the heat of reaction of the sample. The thermal resistance and the heat capacity effects of the sample, however, should be considered to accurately represent the mathematical model of a DSC.

Many binary organic mixtures show simple eutectic solid–liquid equilibrium (SLE) phase diagrams. The DSC curves of simple eutectic phase diagram superimpose eutectic and solid–liquid transition reaction. Theoretically, the isothermal reaction (eutectic peak) in an ideal equilibrium DSC curve is a delta function. The actual eutectic peak shows, however, a broad distribution due to the thermal resistance of the sample and the finite scanning rate of the DSC apparatus. The actual curve

* Corresponding author. Tel.: +886-2-2363-5230; fax: +886-2-2362-3040.

E-mail address: ypchen@ccms.ntu.edu.tw (Y. -P. Chen)

0009-2509/00/$ - see front matter
PII: S0009-2509(99)00593-X

Nomenclature

c_R	heat capacity of the reference cell
c_S	heat capacity of the sample cell
f	fractional transformation
f_E	eutectic fraction
f_L	fraction of the liquid-phase
f_S	fraction of the solid-phase
q	thermal energy add to the sample cell
h	heat of reaction
ΔH^f	molar heat of fusion
ΔH_E	energy released at eutectic point
ΔH_A	energy released above eutectic point
I	ideal or imaginary DSC curve
n	number of time intervals or experimental data points
O	measured DSC curve
R	thermal resistance
Rc_S	time constant
t	time
T_E	eutectic temperature
T_L	liquidus temperature
T_m	melting temperature
T_P	temperature of the source of thermal energy
T_R	temperature of the reference cell
T_S	temperature of the sample cell
T^{Calc}	calculated liquidus temperature
T^{Expt}	measured liquid temperature
x_0	initial uniform composition
x_E	eutectic composition
x_L	liquid-phase composition
x_S^*	solid-phase composition in the solid–liquid interface
Z	instrumental function
Obj	objective function

Greek letters

γ	activity coefficient
δ	Delta function
τ	time
Λ	Wilson model coefficient

approaches to the ideal result as the amount of sample or the scanning rate becomes extremely small. This limiting approach is taken as the thermal equilibrium method (TEM). Matsuoka and Ozawa (1989) regarded the DSC apparatus as a black box that transforms the ideal thermal response through the convolution method (CM) to an actual output. Shibuya, Suzuki, Yamaguchi, Arai and Saito (1993) presented the deconvolution method (DM) and directly obtained the ideal DSC curve from a set of linear equations and the Gauss–Seidel method. The transfer function (or the instrumental function) was taken as a characteristic property of the measuring equipment and was used to determine the ideal curve (original input) of the experimental sample. Matsuoka and Ozawa (1989) and Shibuya et al. (1993) used a triangle-type equation as the transfer function for a specific experimental system. For an ideal DSC peak of an isothermal reaction, the convolutional integration of this delta function and the equipment transfer function gives the transfer function itself. Thus, we employed in this study the actual DSC curve of a pure component as the transfer function. No assumption for the specific shape of the transfer function is required. The ideal DSC curve of an organic mixture was then determined using the deconvolution method.

In the solid–liquid-phase equilibria, the fraction of transformation is always regarded as an important property of materials. It was used to evaluate the kinetics of reaction, the phase transformation rate or the solidification curves (Speyer, Richardson & Risbud, 1986; Hammami & Mehrotra, 1992; Chen, Huang & Lin, 1995; Chen & Huang, 1996). The fractional transformation was determined by the simple lever rule, the Scheil model (Flemings, 1974), the image analysis method for quenched sample (Chen & Chang, 1991), or the measurement of electrical potential difference (Kiuchi & Sugiyama, 1994). It is difficult to directly obtain the solid (or liquid) fraction of semi-solid sample from experimental measurement. In this study, we determined the fraction of transformation by calculating the fractional heat of melting, which was integrated by employing the Gray's model for a deconvoluted DSC measurement.

The experimental SLE results of three binary organic mixtures are reported in this study. The Wilson and the UNIFAC models are used to correlate or predict the equilibrium curves. Finally, we demonstrate that the prediction of the SLE curve and the eutectic point gives satisfactory agreement to the experimental results by applying the deconvolution technique, the Gray's model and the modified fractional transformation approach.

2. Experimental

The SLE data of binary organic mixtures were measured by Perkin-Elmer DSC-7 equipment. The organic samples were weighted in a total amount of 100 g and ground to obtain uniform mixtures. All measurements were made with samples of about 5 mg sealed in a high-pressure copper container made by DuPont Co. The accuracy of the balance (Mettler, AT200) is ± 0.1 mg.

Table 1
Comparison of the measured onset temperatures and equilibrium melting temperatures of pure components

Component	T_m (K)	Measured onset temperature (K)
Benzoic acid	395.4[a]	395.6
2-Aminobenzoic acid	418.0[a]	418.6
1-Naphthol	369.0[a]	369.1
In	429.7[a]/429.8[b]	429.6
Zn	692.5[a]/692.7[b]	692.7

[a]CRC Handbook of Chemistry and Physics, 78th Edition (1997).
[b]Hohne (1991).

The DSC was purged with nitrogen gas at a rate of 0.01 l/min. A blank test was carried out at a scanning rate of 10 K/min from 323.15 to 473.15 K and a straight baseline was obtained by adjusting the power output ratio between two micro-furnaces. The calibration of the DSC was made using high-purity indium and zinc at various scanning rates.

The binary organic samples were heated quickly to a temperature above the melting point of the mixture. After the sample was melted, the temperature was cooled to 323.2 K and maintained at this temperature for 30 min. The DSC experiments were then carried out at a specified heating rate of 10 K/min. The accuracy of the measured temperature is estimated to be ± 0.2 K.

Three organic compounds of benzoic acid, 2-amino benzoic acid and 1-naphthol were purchased from Merck Co. The purity of these samples is better than 99 mass%. The melting temperatures of pure compounds are measured in this study and the comparison of the measured values with literature data is listed in Table 1.

3. Theoretical models and correlation

3.1. The mathematical description of the DSC

DSC is a technique which measures the thermal difference between the sample cell and the reference cell under a same scanning rate (Wendlandt, 1986). A heat transfer modeling was proposed by Gray (1968) to describe the heat flow in a DSC cell:

$$\frac{dh}{dt} = c_s\frac{dT_s}{dt} - \frac{dq_s}{dt}, \tag{1}$$

where h is the heat generation during the phase transformation reaction, c_s is the heat capacity of the sample, T_s is the sample temperature, and q_s is the thermal energy added to the sample. According to the Newton's cooling law, the thermal energy flow rate is proportional to the temperature difference divided by the thermal resistance:

$$\frac{dq_s}{dt} = \frac{T_p - T_s}{R}, \tag{2}$$

where T_p is the temperature of the thermal energy source, and R is the thermal resistance of the path between the thermal energy source and the cell. Since there is no heat generation occurring in the reference cell, the balance equation for the reference cell becomes (provided that there exists identical heat resistance for the two cells and there is no heat generation in the reference cell)

$$0 = c_r\frac{dT_r}{dt} - \frac{dq_r}{dt}, \tag{3}$$

$$\frac{dq_r}{dt} = \frac{T_p - T_r}{R}. \tag{4}$$

Subtracting Eq. (3) from Eq. (1), we obtain the difference for the heat generation rates of the two cells:

$$\frac{dh}{dt} = c_s\frac{dT_s}{dt} - c_r\frac{dT_r}{dt} + \frac{T_s - T_r}{R}. \tag{5}$$

Rearranging the above equations, we have

$$\begin{aligned}\frac{dh}{dt} &= c_s\frac{dT_s}{dt} - c_s\frac{dT_r}{dt} + c_s\frac{dT_r}{dt} - c_r\frac{dT_r}{dt} + \frac{T_s - T_r}{R}\\ &= c_s\frac{d(T_s - T_r)}{dt} + (c_s - c_r)\frac{dT_r}{dt} + \frac{T_s - T_r}{R}\\ &= -\frac{dq}{dt} + (c_s - c_r)\frac{dT_r}{dt} - Rc_s\frac{d^2q}{dt^2}\end{aligned} \tag{6}$$

where

$$\frac{dq}{dt} = \frac{T_r - T_s}{R}, \tag{7}$$

dq/dt is the power difference (or heat flow) between the sample and the reference cells, and it is directly measured by the DSC. dT_r/dt is the constant scanning rate of the experiment.

Before the phase transformation, there is no heat generation ($dh/dt = 0$), and the baseline is adjusted to be horizontal ($d^2q/dt^2 = 0$). The constant offset in the DSC curve is

$$\frac{dq}{dt} = (c_s - c_r)\frac{dT_r}{dt} \tag{8}$$

Eliminating the baseline effect, the Gray's model becomes

$$\frac{dh}{dt} = -\frac{dq}{dt} - Rc_s\frac{d^2q}{dt^2}. \tag{9}$$

At the end of phase transformation, dq/dt reaches its maximum value, and there is no heat generation after this point. The DSC curve then approaches to the baseline

according to an exponential decay equation:

$$\frac{dq(t)}{dt} = \left(\frac{dq}{dt}\right)_{max} \exp(-t/Rc_s), \tag{10}$$

where Rc_s is taken as the time constant for a DSC measurement system.

3.1.1. The deconvolution method

A DSC apparatus is regarded as a black box that transforms imaginary thermal response into actual output by assuming a specific instrumental function (Matsuoka & Ozawa, 1989):

$$o(t) = \int_0^t i(\tau)\cdot z(t-\tau)\,d\tau = \int_0^t i(t-\tau)\cdot z(\tau)\,d\tau, \tag{11}$$

where $o(t)$ is a measured DSC curve, $i(t)$ is an ideal DSC curve at a phase equilibrium condition, and $z(t)$ is the instrumental function. Theoretically, the ideal DSC curve can be determined by employing an inverse Fourier transformation.

The ideal DSC curve can also be solved by the deconvolution method from a set of linear equations (Shibuya et al., 1993). In this study, we take the ideal DSC curve I and the actual DSC curve O as column matrixes of n elements. Each element in the matrix represents the DSC data at various time intervals. The instrumental function Z is then represented by an $n\times n$ matrix:

$$Z(n\times n)\cdot I(n\times 1) = O(n\times 1); \tag{12}$$

Eq. (12) is rearranged for diagonal domination. It is then solved using the Gauss–Seidel method and suitable relaxation factor to obtain a stable and converged solution for the ideal DSC curve.

The ideal DSC curve of a pure compound is a delta function. Thus, the instrumental function is the actual DSC output result for a pure reference compound:

$$\int_0^t \delta(\tau)\cdot z(t-\tau)\,d\tau = z(t). \tag{13}$$

In this study, the instrumental function was determined from a DSC experiment of pure indium. The ideal DSC curves for three organic binary mixtures were solved employing this instrumental function and the deconvolution method.

3.2. The fractional transformation

The fractional transformation is defined as the fraction of the mixture that is liquefied. It is equal to the ratio of the heat generated during the time interval of the phase transition process to the total heat released under the liquidus temperature. The fractional transformation was calculated using the Gray's model:

$$f_L = \int_0^t \frac{dh(t)}{dt}dt/\Delta H = \int_0^t \left(-\frac{dq(t)}{dt} - Rc_s\frac{d^2q(t)}{dt^2}\right)dt/\Delta H. \tag{14}$$

At the end of a DSC experiment, the measured heat flow approaches to zero. The overall integration result of the time constant term thus becomes zero. This implies that the time constant term does not affect the total heat measured, but does affect the shape of phase transformation curve. The total heat of phase transformation was evaluated by

$$\Delta H = \int_0^\infty \frac{dh(t)}{dt}dt = \int_0^\infty -\frac{dq(t)}{dt}dt. \tag{15}$$

The solid–liquid equilibrium phase boundary can be determined directly from the DSC experimental results where the solid–liquid transition temperatures are recorded. It can also be evaluated from the calculated fractional transformation data. The simplest models for describing the relationship between the fractional transformation and the composition of phase boundary are the equilibrium lever rule and the Scheil model.

The Scheil model considers the composition distribution in the solid phase and is also called the non-equilibrium lever rule. The assumptions of the Scheil model are: (1) diffusion in the solid phase is negligible; (2) local equilibrium is maintained at the solid–liquid interface; (3) uniform liquid composition; and (4) equal solid and liquid densities. With the Scheil's assumptions, a mass balance is expressed as

$$(x_L - x_S^*)df_S = f_L dx_L, \tag{16}$$

where f_S is the fraction of solid phase, x_L and x_S^* denote the liquid- and the solid-phase composition at the solid–liquid interface. Combine the phase boundary conditions, the expression of Scheil model becomes

$$\int_{x_0}^{x_L} \frac{1}{x_L - x_S^*}\,dx_L + \int_1^{f_L} \frac{1}{f_L}\,df_L = 0, \tag{17}$$

where x_0 is the initial uniform composition of the sample. Eq. (17) is similar to the Rayleigh equation used in Matsuoka and Ozawa (1989) for calculation of the equilibrium mole fraction. For the simple eutectic SLE, there is no solid solution, and x_S^* becomes zero. Eq. (17) thus reduces to the equilibrium lever rule ($x_L = x_0/f_L$). The DSC curve measured by Perkin-Elmer DSC 7 and was deconvoluted to obtain the ideal DSC curve by Eq. (12). The fractional transformation data was calculated by the Gray's model and the ideal DSC curve. The solid–liquid phase boundary was then determined according to the equilibrium lever rule and these liquid fraction results.

3.3. Thermodynamic correlation

The solid–liquid equilibrium is represented by the following equation:

$$\ln(\gamma_i x_i) = -\frac{\Delta H^f}{RT_{m,i}}\left(\frac{T_{m,i}}{T}-1\right) - \frac{\Delta c_p}{R}\left(\ln\frac{T_{m,i}}{T}-\frac{T_{m,i}}{T}+1\right), \quad (18)$$

where the melting temperature T_m, molar heat of fusion ΔH^f, heat capacity c_p, and the activity coefficient γ are required to determine the equilibrium composition x. The activity coefficients are determined from an excess Gibbs free energy model. The Wilson equation (Wilson, 1964) was employed in this study to correlate the experimental results:

$$\frac{G_{ex}}{RT} = -x_1\ln(x_1+\Lambda_{12}x_2) - x_2\ln(x_2+\Lambda_{21}x_1), \quad (19)$$

$$\ln\gamma_1 = -\ln(x_1+\Lambda_{12}x_2) + x_2\left(\frac{\Lambda_{12}}{x_1+\Lambda_{12}x_2} - \frac{\Lambda_{21}}{\Lambda_{21}x_1+x_2}\right) \quad (20)$$

$$\ln\gamma_2 = -\ln(x_2+\Lambda_{21}x_1) - x_1\left(\frac{\Lambda_{12}}{x_1+\Lambda_{12}x_2} - \frac{\Lambda_{21}}{\Lambda_{21}x_1+x_2}\right). \quad (21)$$

The following objective function was minimized to obtain the optimal binary parameters Λ_{12} and Λ_{21} for each binary mixture:

$$Obj = \sum(\gamma_i^{cal} - \gamma_i^{exp})^2. \quad (22)$$

The SLE curves were also predicted by the group contribution UNIFAC equation (Fredenslund, Jones & Prausnitz, 1975). The calculated results were compared with experimental data to test the applicability of the activity coefficient models.

4. Results and discussion

In this study, high-purity indium and zinc were used to calibrate the DSC equipment. Fig. 1 shows the DSC results for pure indium at various scanning rates. It is observed that as the scanning rate decreases, an ideal peak is approached. The exponential decay curves shown in Fig. 1 demonstrate that the Gray's model with a time constant Rc_s is appropriate to describe the DSC behavior. The thermal equilibrium melting temperatures for indium and zinc by extrapolating to a zero scanning rate in this study are 429.6 and 692.7 K, respectively. The measured heats of fusion in this study for indium and zinc

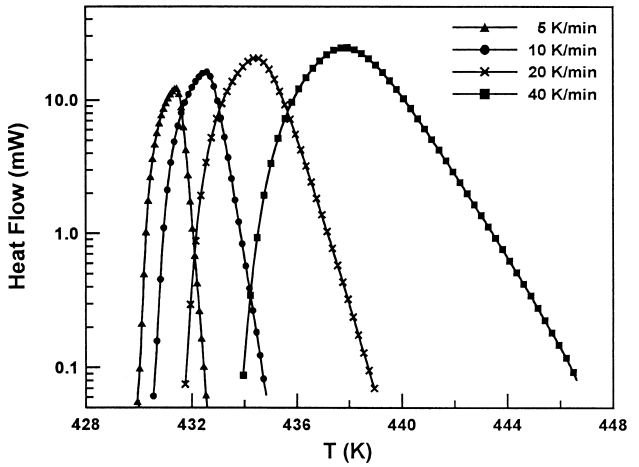

Fig. 1. Measured DSC curves from different scanning rates of pure indium.

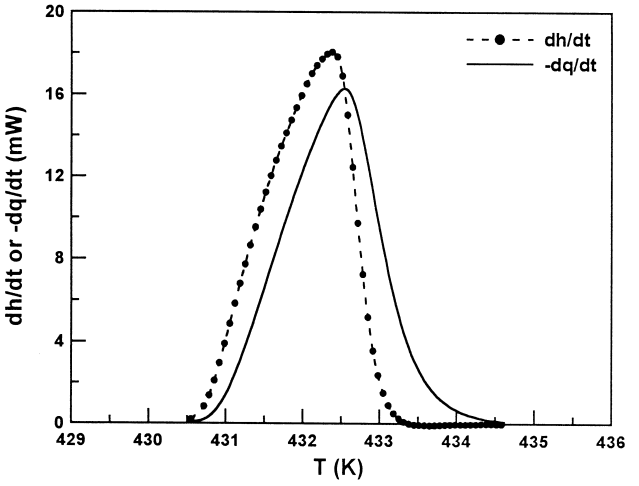

Fig. 2. Comparison of measured heat flow curve ($-\mathrm{d}q/\mathrm{d}t$) and calculated heat generation curve ($\mathrm{d}h/\mathrm{d}t$) of pure Indium at scanning rate 10 K/min.

are 28.6 ± 0.2 and 111.4 ± 0.5 J/g, respectively. These results are in good agreement with literature data (Hohne, 1991). Fig. 2 shows the measured DSC heat flow curve ($-\mathrm{d}q/\mathrm{d}t$) at various temperatures for pure indium using a heating rate of 10 K/min. The calculated heat generation rate curve ($\mathrm{d}h/\mathrm{d}t$) is also presented in Fig. 2. The Gray's model with a time constant term as shown in Eq. (9) was employed in the calculations. The peak of the heat generation rate is sharper than that of the heat flow. These curves have the same overall area but the partial areas under the same temperature are different.

Fig. 3 presents the calculated fractional transformation for pure indium. The dashed curve is the result from the direct integration of the DSC heat flow ($-\mathrm{d}q/\mathrm{d}t$). The solid curve gives the integration results using Eq. (14). The normalized DSC heat flow curve is also shown in

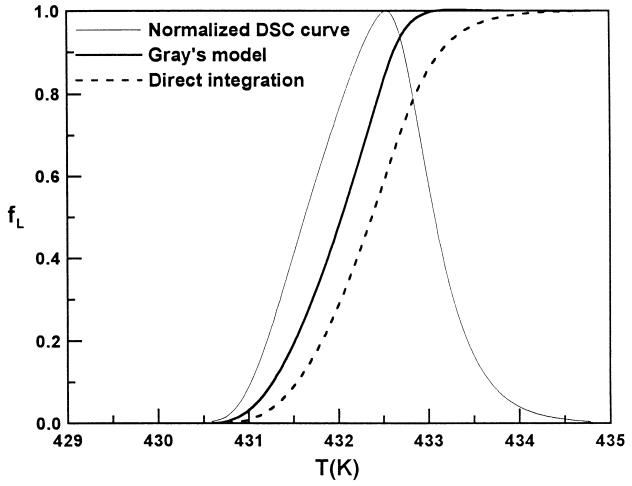

Fig. 3. Calculated fractional transformation curves by using either the Gray's model or the direct integration method for pure Indium (scanning rate 10 K/min).

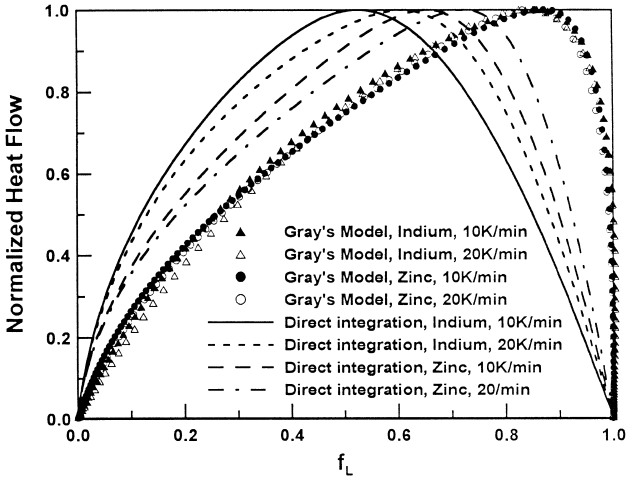

Fig. 4. Comparison of normalized DSC curves against the fractional transformation by the Gray's model and the direct integration method.

Fig. 3. The maximum fractional transformation is 1.0, and this is taken as the end point of phase transformation. It is observed that the integration by employing the Gray's model yields a result closer to a unit-step function for a pure component than that from the direct integration without a time constant term. The end point of the phase transition process determined from the Gray's model is also closer to the DSC result than that from the direct integration.

Fig. 4 shows a plot of the normalized DSC curve against the fractional transformation. Using the DSC heat flow output only and without considering the time constant term, the curves for different pure compounds and scanning rates are individually separated. All curves coincide using the Gray's model with the time constant term. For the isothermal phase transition process, a single ideal curve should be obtained. It is observed from Fig. 4 that the shapes of the DSC curves are affected by the characteristics of the DSC equipment. The results from Figs. 2–4 also demonstrate that the Gray's model with a time constant term effectively represent the DSC behavior and should be used to determine the fractional transformation.

Fig. 5 shows a typical DSC curve of a eutectic mixture. The DSC curve exhibits isothermal eutectic and non-isothermal solid–liquid transition peaks. The eutectic and liquidus temperatures can approximately be obtained from the onset point of the first- and second-peak temperature shown in Fig. 5, respectively. Appreciable errors may exist owing to the non-sharp peak behavior. Matsuoka and Ozawa (1989) used a triangle shape transfer function to solve for the ideal DSC curve from the deconvolution method. Examining the pure component DSC curve (as shown in Fig. 1) with small scanning rate, or the eutectic peak shown in Fig. 5, it is concluded that

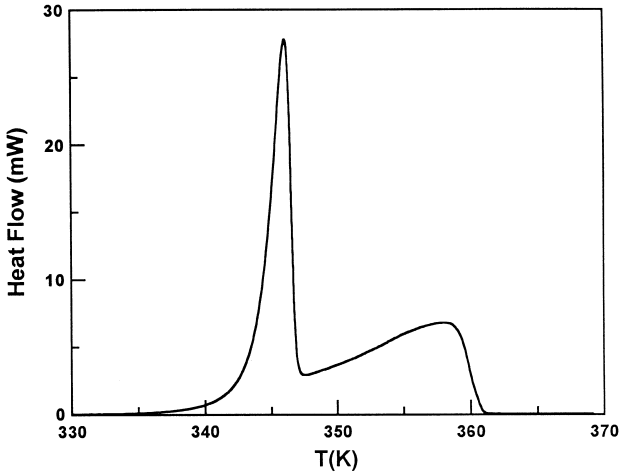

Fig. 5. A typical DSC curve exhibiting isothermal eutectic and solid–liquid transition peaks.

a simple triangle function is not adequate to represent the DSC transfer function. In this study, we employed Eqs. (9) and (12) to evaluate the transfer function matrix $Z(n \times n)$ from the DSC curve of a pure indium component. For the other actual DSC output matrix $O(n \times 1)$, the same instrumental function is used to solve for the ideal DSC matrix $I(n \times 1)$. Fig. 6 shows a typical example for the measured DSC curve of benzoic acid and 1-naphthol binary mixture at a small scanning rate of 4 K/min. The calculated results from the deconvolution method using a transfer function of pure indium are also shown in Fig. 6. It is evident that the deconvoluted results, which yield an ideal DSC curve, approximate well the measured data at a small scanning rate.

Matsuoka and Ozawa (1989) suggested a procedure for confirming the composition of the eutectic point in

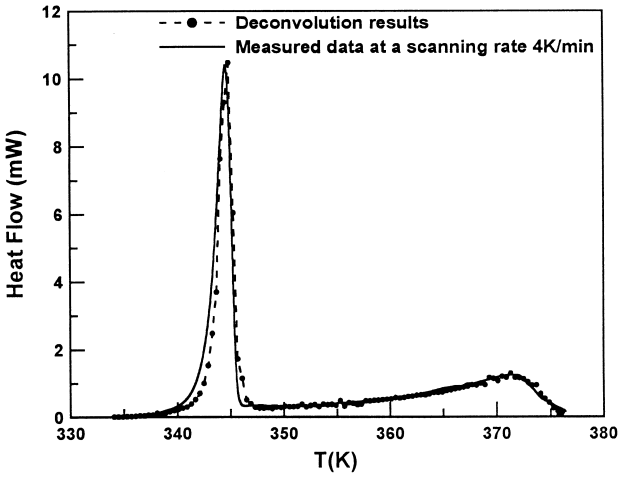

Fig. 6. Comparison of the measured data and the calculated results from the deconvolution method for a binary mixture of benzoic acid and 1-naphthol.

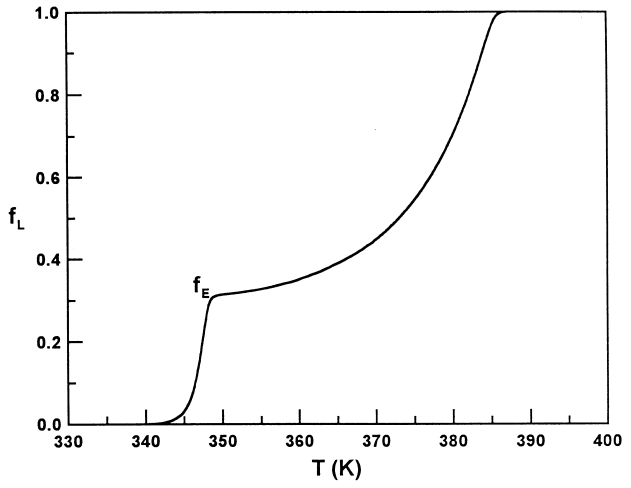

Fig. 7. A typical fraction transformation curve of a simple eutectic mixture.

the solid–liquid equilibrium. The amount of energy released at the eutectic point (ΔH_E) and the total energy released above the eutectic temperature (ΔH_A) was determined at various compositions. The plots of these data at various compositions were used to locate the maximum point of ΔH_E and the minimum point of ΔH_A. The maximum or minimum point determines the eutectic composition. This procedure needs to measure the accurate weight of sample as well as the DSC peak area of the eutectic and the solid–liquid transition reactions. Since the eutectic and the solid–liquid transition peaks separate well only at the point near the pure component due to the superimposed effect, it is difficult to determine accurately the values of ΔH_E and ΔH_A near the eutectic point.

The sample weight used in DTA or DSC is usually small. The confirmation method suggested by Matsuoka and Ozawa (1989) needs accurate sample weight to determine molar transitional enthalpy. To avoid the difficulty of observing the accurate measurement of sample weight and the separated peaks of eutectic and solid–liquid reaction, an easier way to confirm the eutectic point is proposed in this study using the measured eutectic fraction (f_E) data. The eutectic fraction is expressed as

$$f_E = \Delta H_E/(\Delta H_E + \Delta H_A). \quad (23)$$

Fig. 7 shows a typical plot of the fractional transformation curve of a simple eutectic mixture. The fractional transformation represents the reaction fraction of solid–liquid equilibrium transition. As shown in (14), the reaction fraction occurred at any temperature could be determined, and the overall transitional enthalpy is used to eliminate the effect of sample weight. This method is also more accurate than the measurement of electrical potential difference (Kiuchi & Sugiyama, 1994) because the former one is the direct measurement of transitional enthalpy with smaller amount of sample. The eutectic

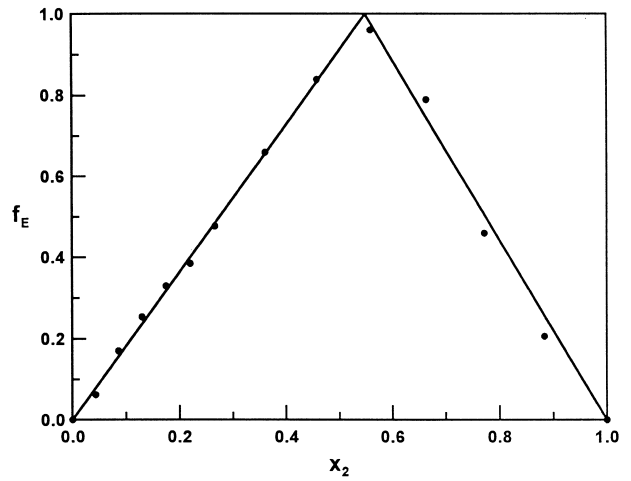

Fig. 8. Eutectic fraction plot for the binary mixture of benzoic acid (1) and 1-naphthol (2) system.

and liquidus temperatures, and the eutectic fraction value (f_E) are easily determined from the plot in Fig. 7. In this study, DSC results for various compositions of binary mixtures were obtained. The corresponding plots for the fractional transformation against temperature were made at each composition. Figs. 8–10 show the plots of the calculated fraction eutectic against composition for the three binary mixtures, respectively. The peak in each triangle shape curve indicates the composition of the eutectic point where the fractional eutectic is unity. These plots show an easier and more accurate way to determine the eutectic point, and avoid any experimental error owing to the weights of small amount of samples, or the difficulty in direct reading from the DSC curve.

The SLE of three binary mixtures of benzoic acid (1) + 1-naphthol (2), benzoic acid (1) + 2-aminobenzoic

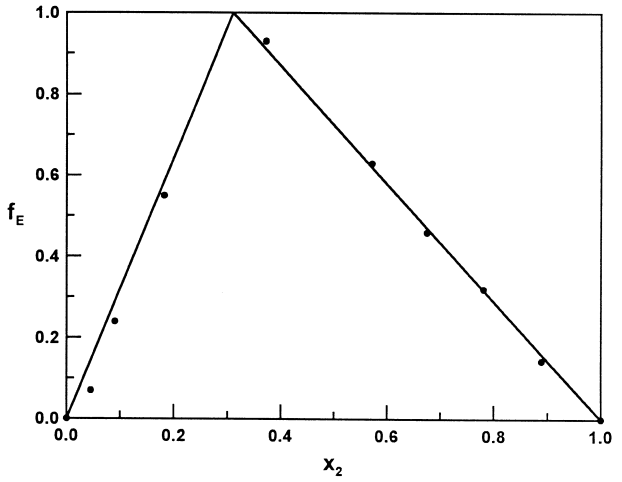

Fig. 9. Eutectic fraction plot for the binary mixture of benzoic acid (1) and 2-aminobenzoic acid (2) system.

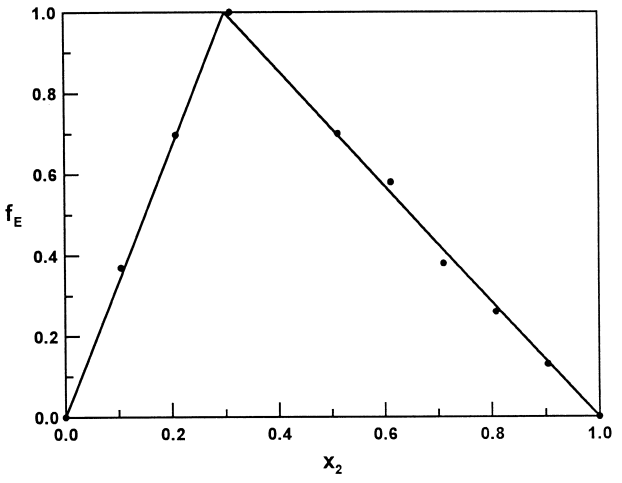

Fig. 10. Eutectic fraction plot for the binary mixture of 1-naphthol (1) and 2-aminibenzoic acid (2) system.

acid (2) and 1-naphthol (1) + 2-aminobenzoic acid (2) were determined by the DSC measurement and theoretical calculations using the Gray's model and the deconvolution method. The solid–liquid equilibrium results are shown in Table 2. Graphical presentations for the three binary systems are shown in Figs. 11–13, respectively. It is demonstrated that deconvolution method and Gray's model provides a suitable approach to measure the simple eutectic SLE. The liquidus curves were also calculated using Eq. (18) with either the Wilson or the UNIFAC activity coefficient model. With two optimally fitted binary parameters for each mixture, the Wilson equation yields satisfactory agreement to the experimental data. The UNIFAC predictions give larger deviation for the binary mixture of benzoic acid (1) + 2-aminobenzoic acid (2), although satisfactory results are

Table 2
Measured solid–liquid equilibrium data for three binary mixtures

x_2	T_L (K)	f_E	x_2	T_L (K)	f_E
Benzoic acid (1) + 1-naphthol (2)					
0.0	395.6	0	0.459	351.8	0.839
0.043	393.7	0.062	0.664	348.6	0.790
0.086	387.6	0.171	0.772	356.1	0.481
0.130	384.8	0.253	0.820	358.3	N/A
0.175	380.0	0.330	0.884	362.4	0.206
0.220	376.5	0.385	0.942	365.9	N/A
0.266	370.6	0.484	1.0	369.1	0
0.361	362.3	0.660			
Benzoic acid (1) + 2-aminobenzoic acid (3)					
0.0	395.6	0	0.571	394.6	0.629
0.090	391.1	0.243	0.675	400.7	0.463
0.182	385.1	0.510	0.781	407.2	0.323
0.276	378.5	N/A	0.889	412.8	0.144
0.373	380.1	0.931	1.0	418.6	0
0.471	387.6	N/A			
1-Naphthol (2) + 2-aminobenzoic acid (3)					
0	369.1	0	0.513	375.5	0.705
0.106	363.2	0.370	0.612	384.1	0.578
0.208	355.1	0.697	0.711	395.2	0.382
0.290	350.0	N/A	0.808	404.0	0.264
0.311	352.1	1.000	0.905	410.0	0.130
0.412	365.1	N/A	1	418.6	0

N/A: not available.

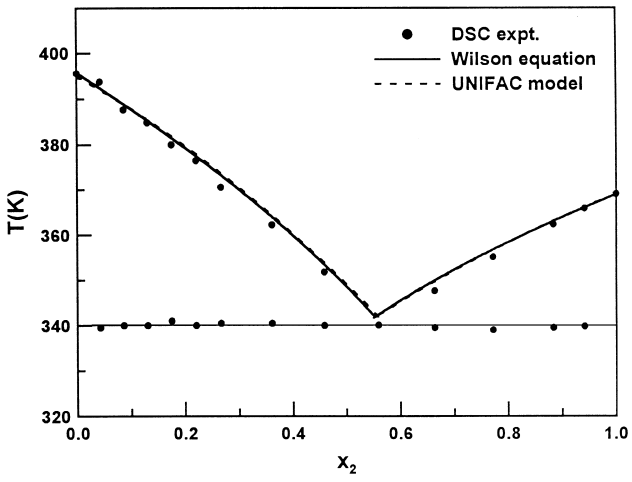

Fig. 11. The measured data and calculated equilibrium curves for the binary mixture of benzoic acid (1) and 1-naphthol (2) system.

obtained for the other two binary systems. The best fitted binary interaction parameters for the Wilson equation and the deviations of regression for three binary systems are presented in Table 3. The comparison of the eutectic compositions and temperatures determined by different methods for three binary mixtures are shown in Table 4. The composition of the eutectic point determined by the

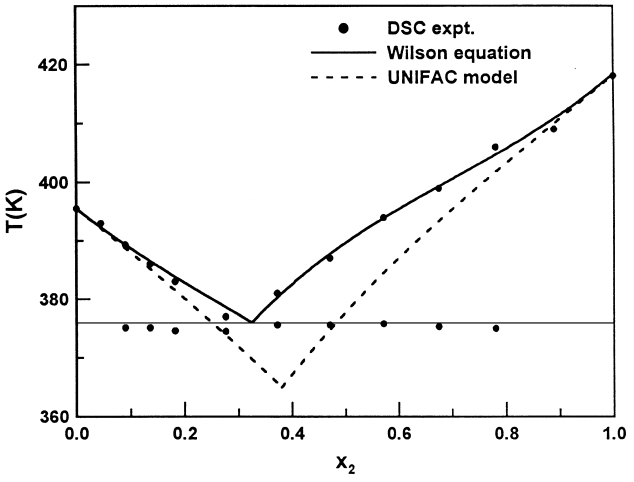

Fig. 12. The measured data and calculated equilibrium curves for the binary mixture of benzoic acid (1) and 2-aminobenzoic acid (2) system.

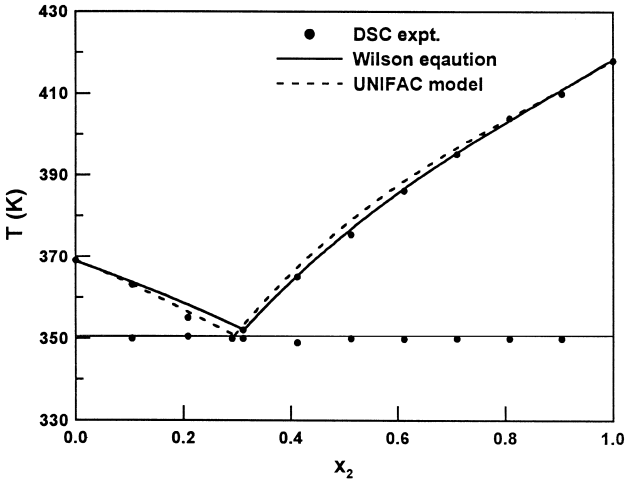

Fig. 13. The measured data and calculated equilibrium curves for the binary mixture of 1-naphthol (1) and 2-aminobenzoic acid (2) system.

Table 3
Results of the fitted binary parameters of the Wilson equation and the deviations of regression

System	Wilson parameters $\Lambda_{12}/\Lambda_{21}$	Deviation σ_T (K)[a]	
		Wilson	UNIFAC
Benzoic acid (1)–1-naphthol (2)	1.5484/0.6326	0.737	0.812
Benzoic acid (1)–2-aminobenzoic acid (2)	0.4984/0.5944	1.132	6.950
1-Naphthol (1)–2-aminobenzoic acid (2)	1.2658/0.6377	1.216	1.320

[a] $\sigma_T\,(K) = \left[\sum_{i=1}^{n} \frac{(T_i^{\mathrm{Calc}} - T_i^{\mathrm{Expt}})^2}{n}\right]^{1/2}$.

Table 4
Comparison of the eutectic point results from different methods for three binary mixtures

Method	x_2	T_E (K)
Benzoic acid (1) + 1-naphthol (2)		
Wilson equation	0.558	341.5
UNIFAC model	0.565	341.7
DSC experiments	0.560	340.1
Fraction method	0.554	N/A
Benzoic acid (1) + 2-aminobenzoic acid (2)		
Wilson equation	0.321	375.9
UNIFAC model	0.392	364.4
DSC experiments	0.314	375.3
Fraction method	0.311	N/A
1-Naphthol (1) + 2-aminobenzoic acid (2)		
Wilson equation	0.311	351.4
UNIFAC model	0.293	350.2
DSC experiments	0.290	350.6
Fraction method	0.291	N/A

N/A: not available.

fraction method is similar to the experimental and the correlated results. The new confirmation method proposed in this study yields an improvement to the previous method of Matsuoka and Ozawa (1989) since the effect of small inaccuracy in the sample weight measurement can be avoided.

The solid–liquid equilibrium phase boundaries were also predicted in this study from the fractional transformation data. The DSC measurements give the heat flow curve dq/dt. Using the deconvolution method, an ideal DSC curve is obtained and the fractional transformation f_L is calculated from Eq. (14). The liquidus composition x_L is then determined by the equilibrium lever rule ($x_L = x_0/f_L$). Since the DSC records continuously the heat flow data, x_L values are calculated at various temperatures for a given initial composition of the sample. The liquidus-phase boundary is thus predicted from a simple DSC measurement. Only one DSC experiment for an initial composition on either side of the eutectic point is required. The phase boundaries calculated from the liquid fraction data are shown in Figs. 14–16. It is demonstrated in these figures that the

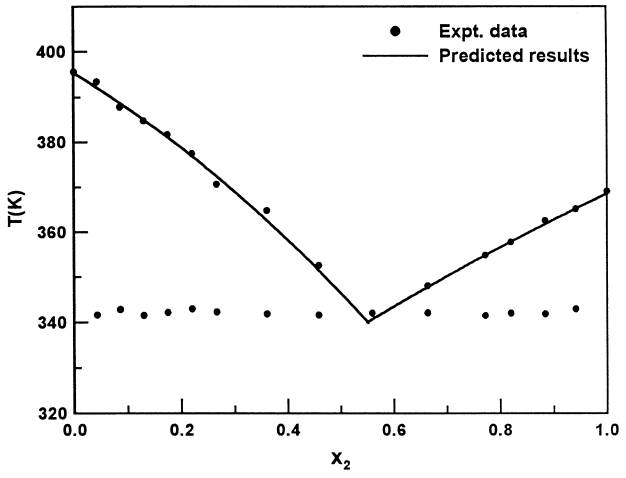

Fig. 14. Predicted results of the solid–liquid-phase boundary for the binary mixture of benzoic acid (1) and 1-naphthol (2) system.

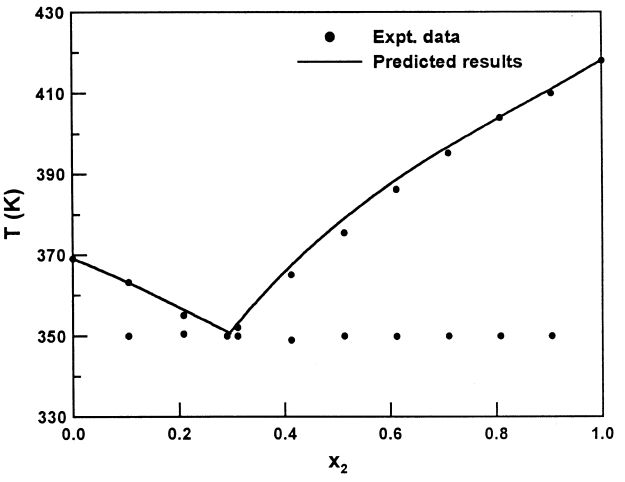

Fig. 16. Predicted results of the solid–liquid-phase boundary for the binary mixture of 1-naphthol (1) and 2-aminobenzoic acid (2) system.

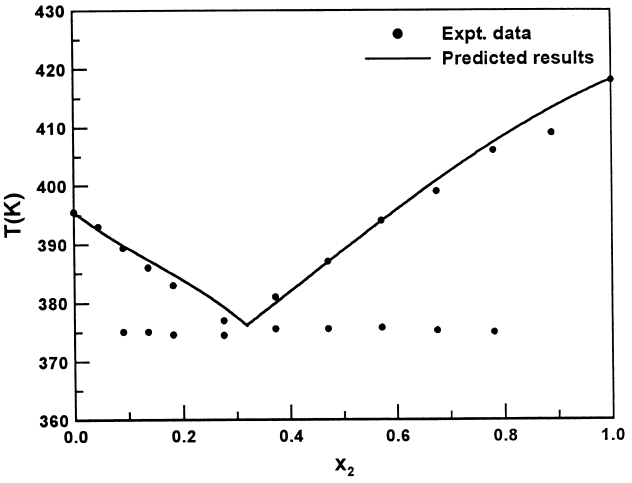

Fig. 15. Predicted results of the solid–liquid-phase boundary for the binary mixture of benzoic acid (1) and 2-aminobenzoic acid (2) system.

predicted phase boundaries agree well with the experimental results. The eutectic temperatures and compositions are satisfactorily predicted from only two experimental measurements for each binary mixture.

5. Conclusions

SLE for three binary mixtures of benzoic acid, 1-naphthol and 2-amino benzoic acid have been measured from the DSC experiments. The instrumental function was determined from the pure component DSC measurement. The deconvolution method was used to obtain the ideal DSC curves, and the Gray's model was used to eliminate the effect of heat resistance of the sample. The fractional transformations were evaluated by employing the Gray's model. It is demonstrated that the Gray's model is suitable to represent the DSC behavior. An easy and accurate way to confirm the eutectic point is proposed by employing the fractional transformation method. The experimental data are well correlated by the Wilson model with its optimally fitted binary parameters. The phase boundaries of SLE are also satisfactorily predicted with the fractional transformation results from two experimental measurements for each binary system.

Acknowledgements

The authors are grateful to the National Science Council for providing the financial support for this study.

References

Chen, S. W., & Chang, Y. A. (1991). Application of thermodynamic models to the calculation of solidification paths of Al-rich Al-Li alloys. *Metallurgical Transactions A*, *22A*, 267–271.

Chen, S. W., & Huang, C. C. (1996). Solidification curves of Al–Cu. *Al–Mg and Al–Cu–Mg alloys. Acta Metallurgica*, *44*, 1955–1965.

Chen, S. W., Huang, C. C., & Lin, J. C. (1995). The relationship between the peak of DTA curves and the shape of a phase diagram. *Chemical Engnieering Science*, *50*, 417–431.

Ciach, R., Kapturkiewicz, W., Wolczynski, W., & Zahra, A. M. (1992). Computer simulation of thermal analysis in heat-flux DSC applied to metal solidification. *Journal of Thermal Analysis*, *38*, 1949–1957.

Flemings, M. C. (1974). *Solidification processing*. New York: McGraw-Hill.

Floter, E., Hollanders, B., de Loos, T. W., & de Swaan Arons, J. (1997). Ternary system (n-heptane + docosane + tetracosane): the solubility of mixtures of docosane and tetracosane in heptane and data on solid–liquid and solid–solid equilibria in the binary subsystem (docosane + tetracosane). *Journal of Chemical Engineering Data*, *42*(3), 562–565.

Fredenslund, A., Jones, R. L., & Prausnitz, J. M. (1975). Group-contribution estimation of activity coefficients in nonideal liquid mixtures. *A.I.Ch.E. Journal*, *21*, 1086–1098.

Frezzotti, D., Bonifaci, L., Cavalca, G., Malaguti, E., & Ravanetti, G. P. (1993). Solid–liquid equilibrium studies on ε-caprolactam-oligomers system. *Fluid Phase Equilibria*, *83*, 399–406.

Gray, A. P. (1968). *Analytical chemistry* (pp. 209–218). NY: Plenum Press.

Hammami, A., & Mehrotra, A. K. (1992). Non-isothermal crystallization kinetics of *n*-paraffins with chain lengths between thirty and fifty. *Thermochimica Acta*, *211*, 137–153.

Hammami, A., & Mehrotra, A. K. (1995). Liquid–solid–solid thermal behaviour of n-$C_{44}H_{90}$ + n-$C_{50}H_{102}$ and n-$C_{25}H_{52}$ + n-$C_{28}H_{58}$ paraffinic binary mixtures. *Fluid Phase Equilibria*, *111*, 253–272.

Hemminger, W. F., & Sarge, S. M. (1991). The baseline construction and its influence on the measurement of heat with differential scanning calorimetry. *Journal of Thermal Analysis*, *37*, 1455–1477.

Hohne, G. W. H. (1991). Remarks on the calibration of differential scanning calorimeters. *Journal of Thermal Analysis*, *37*, 1987–2000.

Jakob, A., Joh, R., Rose, C., & Gmehling, J. (1995). Solid–liquid equilibria in binary mixtures of organic compounds. *Fluid Phase Equilibria*, *113*, 117–126.

Kiuchi, M., & Sugiyama, S. (1994). A new method to detect solid fractions of mushy/semi-solid metals and alloys. *Annals of the CIRP*, *43*, 271–274.

Matsuoka, M., & Ozawa, R. (1989). Determination of solid–liquid phase equilibria of binary organic systems by differential scanning calorimetry. *Journal Crystal Growth*, *96*, 596–604.

Santilli, N., Filippis, P. D., & Chianese, A. (1994). Solid–liquid phase diagram of the binary system benzil + 2,2-dimethoxy-1,2-diphenylethanone. *Journal Chemical Engineering Data*, *39*, 179–180.

Sarge, S. M., Bauerecker, S., & Cammenga, H. K. (1988). Calorimetric determination of purity by simulation of DSC curves. *Thermochimica Acta*, *129*, 309–324.

Shibuya, H., Suzuki, Y., Yamaguchi, K., Arai, K., & Saito, S. (1993). Measurement and prediction of solid–liquid phase equilibria of organic compound mixtures. *Fluid Phase Equilibria*, *82*, 397–405.

Smith, P., & Pennings, A. J. (1974). Eutectic crystallization of pseudo binary systems of polyethylene and high melting diluents. *Polymer*, *15*, 413–419.

Speyer, R. F., Richardson, B. C., & Risbud, S. H. (1986). Nonlinear regression analysis of superimposed DSC crystallization peak. *Metallurgical Transactions A*, *17*, 1479–1481.

Wendlandt, W.W. (1986). Thermal analysis, 3rd ed. New York: Wiley-Interscience.

Wilson, G. M. (1964). Vapor–liquid equilibrium. XI: A new expression for the excess free energy of mixing. *Journal of American Chemical Society*, *86*, 127–130.